Low temperature decoherence and relaxation in charge Josephson junction qubits

Alex Grishin, Igor V. Yurkevich, and Igor V. Lerner

School of Physics and Astronomy, University of Birmingham (UK)

1 Introduction

Research interest in controllable two level systems, which have been enthusiastically called quantum bits or qubits, has grown enormously during the last decade. Behind a huge burst of activity in this field stands an idea of what is possible in principle but extremely difficult to achieve instrumentally - the fascinating idea of quantum computing. The very principle of quantum superposition allows many operations to be performed on a quantum computer in parallel, while an ordinary 'classical' computer, however fast, can only handle one operation at a time. The enthusiasm is not held back by the fact that exploiting quantum parallelism is by no means straightforward, and there exist only a few algorithms (e.g., [1, 2]) for which the quantum computer (if ever built) would offer an essential improvement in comparison with its 'classical' counterpart. Even if other uses of quantum computing prove limited (which might or might not be the case), its existence would most certainly lead to a breakthrough in simulations of real physical many-particle systems.

Whether or not the ultimate goal of building a working quantum computer is ever achieved, both experimental and theoretical studies of properties of single or entangled qubits are flourishing. One of the most compelling reasons for this is an exciting overlap of the possibility of a future technological breakthrough and the reality of research in fundamentals of quantum mechanics. There exist various experimental realisations of the qubit, amongst which solid state qubits are of particular interest as they provide one of the most promising routes to implementing a scalable set of qubits, which is one of the minimal requirements for implementing quantum computations. However, any solid state qubit, albeit representing effectively a two-level system, comprises a huge number of internal degrees of freedom whose unavoidable coupling to the environment leads to loss of coherence. Quantum computations require a set of fully or at least partially entangled states on which some unitary operations are performed. Decoherence would make evolution of states non-unitary and would lead to the loss of entanglement between the states. Thus, the

loss of coherence before a sufficient amount of quantum operations was performed would be the major impediment in using solid-state qubits in quantum computations. It is believed that tens of thousands of unitary operations are required for quantum computation to become a reality [3] so that sufficiently long decoherence times (much longer than those currently archived in the best solid state qubits) should be achieved experimentally. It necessitates a better theoretical understanding of realistic mechanisms of decoherence.

In these lectures, after illustrating in a simple way the main features of decoherence in a generic qubit coupled to the environment (Section 2), we will consider onset of decoherence in one particular realisation of qubit, namely charge Josephson junction (JJ) qubit. First, we will describe briefly what is the JJ qubit (Section 3) and then focus on a mechanism widely believed to be responsible for one of the main channels of decoherence for the charge JJ qubit, namely its inevitable coupling to fluctuating background charges (Section 4). This model has been thoroughly investigated in all regimes [4–7] and has a tutorial advantage of being exactly solvable within a fully quantum approach [7] and showing a rich variety of different regimes with a non-trivial dependence on temperature and on (unfortunately ill known experimentally) the strength of coupling between the qubit and the fluctuating charges.

In Section 5 we will offer a solution for decoherence rate in this model which is formally exact at an arbitrary temperature T. In the 'high-T regime' (which could still correspond to rather low temperatures), the decoherence rate saturates and becomes T-independent, while at low temperature it turns out to be linear in T and behave non-monotonically as a function of the coupling strength between qubit and the environment. In conclusion we will also consider the relaxation rate, albeit only perturbatively with respect to the coupling strength, and demonstrate that the model can qualitatively explain the experimentally observed [8] quasi-linear behaviour of the spectral density of noise with humps at certain frequencies.

2 Coupling to the environment and decoherence

Before considering a realistic solid-state qubit, we start with illustrating what is the loss of coherence in a generic qubit. Such a qubit is a two-level system so that its Hamiltonian can be mapped to that of spin $\frac{1}{2}$ and written

$$\hat{H}_0 = \tfrac{1}{2} B_z \hat{\sigma}_z - \tfrac{1}{2} B_x \hat{\sigma}_x \,. \tag{1}$$

where $\mathbf{B}$ is an effective 'magnetic field' (measured here in energy units). States of the qubit can be described in terms of its density matrix,

$$\hat{\rho}(t) = \sum_{i,j=\uparrow,\downarrow} |i\rangle \, \rho_{ij}(t) \, \langle j| \,. \tag{2}$$

When the qubit (or any system) is in a pure state, one can always find a basis where $\hat{\rho} = \sum_i |i\rangle \langle i|$. In any other (rotated) basis, the density matrix of a pure state obeys $\hat{\rho}^2 = \hat{\rho}$. In a rotated basis, the density matrix performs a unitary evolution described by the Heisenberg equation of motion,

$$\frac{\partial \hat{\rho}(t)}{\partial t} = -i \left[\hat{H}_0, \hat{\rho}(t) \right] , \qquad (3)$$

whose solution is $\hat{\rho}(t) = \hat{U} \hat{\rho}(0) \hat{U}^\dagger$ where in this trivial case the evolution operator $\hat{U} = e^{-iH_0 t}$. In a semiclassical language, such an evolution is convenient
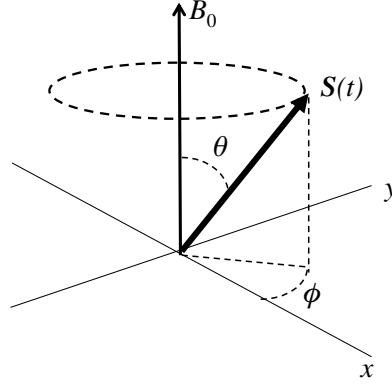

Fig. 1. Bloch representation

to visualise using the Bloch sphere representation, shown in Fig.1. There the spin evolution is parameterised by two angles on a unit sphere, θ and ϕ. For the simple system described by Eqs. (1) – (3) above, such an evolution is simply rotating around z axis, provided that the 'field' $\mathbf{B} = (B_z, 0)$, and the initial state of the spin was diagonal in a different basis. The Bloch angles are related to the density matrix by

$$\rho(t) = \frac{1}{2} \left(1 + \mathbf{S}(t) \cdot \boldsymbol{\sigma} \right) . \qquad (4)$$

An inevitable coupling to the environment (bath) can be schematically described by the Hamiltonian

$$\hat{H} = \hat{H}_0 + \hat{V}_{\text{coupl}} + \hat{H}_{\text{bath}} . \qquad (5)$$

Now it is the full density matrix of the qubit + bath which obeys the Heisenberg equation of motion. As we are interested in states measured on the qubit, we need to introduce a so called 'reduced' density matrix, $\hat{\rho}^q = \text{Tr}_{\text{bath}} \hat{\rho}$ where the trace is taken over all the bath states with the proper Gibbs weight. We will describe a consistent way of performing such a trace in Section 5. Here we

want just to illustrate how the coupling to the environment makes the time evolution non-unitary and leads to the loss of coherence.

Let us consider a model in which there is a minimal, so called longitudinal coupling of the qubit to the bath,

$$V_{\text{coupl}} = \hat{X}\hat{\sigma}_z \,. \tag{6}$$

Let us further assume that the qubit was prepared in a pure state but in a different basis, so that its density matrix has both diagonal and off-diagonal elements,

$$\hat{\rho} \equiv \begin{pmatrix} \rho_{11} & \rho_{12} \\ \rho_{21} & \rho_{22} \end{pmatrix} = \begin{pmatrix} n & f \\ f^* & 1-n \end{pmatrix} \,,$$

with $|f|^2 = n - n^2$ at $t = 0$ assuming that the qubit was prepared in a pure state, $\hat{\rho}^2 = \hat{\rho}$. Let finally switch off the x component of the 'magnetic field' $\mathbf{B}$. In the absence of coupling, the spin that represents our qubit on the Bloch sphere of Fig. 1 would simply rotate at a constant frequency $\omega_0 \propto B_z$ around z axis. The longitudinal coupling effectively introduces and additional, fluctuating time dependent component of the field, $B_z(t)$. This fluctuating field results from the thermal noise in the bath and inevitably destroys coherence as we will now show.

The spin rotation is described in a semiclassical language by the Landau-Lifshitz equation,

$$\frac{d\mathbf{S}}{dt} = \mathbf{S} \times \mathbf{B} \,.$$

In the absence of the transverse component of the magnetic field, the diagonal elements of the density matrix, related to $\mathbf{S}$ by Eq. (4), remain constant. In the presence of the environment-induced time-dependent component of the longitudinal magnetic field, $\mathbf{S}$ rotates with a changing frequency resulting in the off-diagonal elements of $\hat{\rho}$ acquiring the following time-dependence:

$$\rho_{12}(t) = \tfrac{1}{2}\left(S_x + iS_y\right) = \rho_{12}(0)e^{i\omega_0 t + i\int_0^t B(\tau)d\tau} \tag{7}$$

The contributions due to the fluctuating field, $B_z(t)$, should be averaged over time. It is natural to assume that fluctuations of B_z are Gaussian, as they are due to an very large number of degrees of freedom in the bath. For Gaussian fluctuations, one can use the standard averaging formula,

$$\left\langle e^{i\varphi} \right\rangle = e^{-\frac{1}{2}\left\langle \varphi^2 \right\rangle} \,,$$

so that

$$\langle \rho_{12}(t) \rangle = \rho_{12}(0)e^{i\omega_0 t} \left\langle e^{i\int_0^t d\tau B(\tau)} \right\rangle$$

$$= \rho_{12}(0)e^{i\omega_0 t} \exp\left[-\frac{1}{2} \int_0^t d\tau \int_0^t d\tau' \left\langle B(\tau)B(\tau') \right\rangle \right]$$

$$= \rho_{12}(0)e^{i\omega_0 t} \exp\left[-t \int_{-t}^t d\tau \left\langle B(0)B(\tau) \right\rangle \right] \equiv \rho_{12}(0)e^{i\omega_0 t}e^{-\Gamma_2 t} \tag{8}$$

Here we have semi-formally defined the decoherence rate Γ_2 as the rate of relaxation of the off-diagonal part of the density matrix, using that the correlation function of the fluctuating field B_z depends only on the time difference. In this definition, Γ_2 can still be time-dependent. However, for large enough t, longer than the longest relaxation time for thermal noise in the bath which makes B_z fluctuating, Γ_2 should saturate at some limiting value. Thus, making a bit more formal definition, we arrive at

$$\Gamma_2 \equiv \frac{1}{T_2} = \lim_{t\to\infty} \int_{-t}^{t} d\tau \left\langle B(0)B(\tau)\right\rangle = S_B\left(\omega \approx 0\right) , \tag{9}$$

where $S_B(\omega)$ is the noise power spectrum of the fluctuating field B,

$$S_B(\omega) \equiv \int_{-\infty}^{\infty} \left\langle B(0)B(t)\right\rangle e^{-i\omega t}dt . \tag{10}$$

The above calculation should be considered just as an illustration as we have just introduced Gaussian fluctuations of the 'magnetic field' B_z. However, it is very easy both to make this sort of calculations fully quantum-mechanical, and to generalise the model beyond the longitudinal coupling.

To show that the effective coupling to the bath leads to the thermal noise that directly results in the appearance of decoherence given by Eq. (9), one needs to model the bath. The most standard theoretical approach to such modeling and thus to decoherence by the environment is based on spin-boson models [16, 17], where the environment is modelled as a set of harmonic oscillators,

$$\hat{H}_{\text{bath}} = \sum_{\mathbf{k}} \omega_{\mathbf{k}} b_{\mathbf{k}}^{\dagger} b_{\mathbf{k}} \tag{11}$$

The linear coupling in Eq. (6) should be understood as coupling to all the oscillator degrees of freedom,

$$V_{\text{coupl}} = \hat{X}\hat{\sigma}_z \equiv \sum_{\mathbf{k}} \left(\lambda_{\mathbf{k}} b_{\mathbf{k}}^{\dagger} + \text{h.c.}\right) \hat{\sigma}_z \tag{12}$$

The fluctuation-dissipation theorem allows one to express the noise power for the coupling operator $\hat{X}(t)$ (in the interaction picture) as

$$S_X(\omega) = \left\langle X_{\omega}^2\right\rangle + \left\langle X_{-\omega}^2\right\rangle = 2J(\omega)\coth\frac{\hbar\omega}{2T}, \tag{13}$$

where $J(\omega)$ depends on the density of oscillator states, i.e. on the spectrum $\omega_{\mathbf{k}}$ in Eq. (11), and on the coupling $\lambda(\omega)$ in Eq. (12). The decoherence rate is still given by Eq. (9), where $S_X(\omega)$ should be substituted for $S_B(\omega)$. For the most typical, Ohmic model, $J(\omega) \propto \omega$ so that $\Gamma_2 \propto T$. As we will show later, such a linear dependence on temperature is characteristic for a realistic model to be considered later in these lectures, but only for sufficiently low T.

It is straightforward to generalise our considerations beyond the longitudinal model. To this end one should take into account the σ_x-proportional contribution in the qubit action – this would be general enough even if one leaves the coupling as it stands in Eqs. (6) or (12).

3 Charge Josephson junction qubit

Not any two-level system could serve as a qubit. There is a set of requirements that such a system must satisfy in the first place. In 1997 David DiVincenzo [9] formulated five criteria which have to be satisfied by a physical system considered as a candidate for quantum computation, conditions which are widely known as the 'DiVincenzo checklist':

i) One needs well-defined two-state quantum systems (qubits);

ii) One should be able to prepare the initial state of the qubits with sufficient accuracy;

iii) A long phase time coherence is needed, sufficient to allow for a large number ($\sim 10^4$) of coherent manipulations;

iv) Control over the qubit's Hamiltonian is required to perform the necessary unitary transformations;

v) A quantum measurement is needed to read out the quantum information. At the present time any known physical system falls short of the lsit stipulated above. Currently lots of different possibilities of building a quantum computer are investigated including nuclear spins, quantum dots, Josephson junctions, trapped ions, optical lattices, electrons on liquid helium and some others with each of them being quite far from satisfying this or that condition of the above set.

A route which seems to be one of the most promising is to build a system of Josephson junction (JJ) qubits: the qubits which are based on Josephson junctions and utilise the charge and flux degrees of freedom. The main advantages of the superconducting devices involving Josephson junctions are a) a relative easiness to manufacture - the lithographic methods used to fabricate them are well established; b) controllability - gate voltages controlling charge Josephson qubits can be adjusted with a very high degree of accuracy allowing, in particular, the high-fidelity preparation of the initial state of the qubit; and finally c) measurability - the techniques for almost noninvasive measurements which can be used for this type of qubits are quite advanced. It is point iii) in the DiVincenzo checklist - decoherence - which causes the greatest worry for the JJ qubit, as well as for any other realisation of a solid state qubit. We stress again that 'spin up' and 'spin down' states in solid state qubits are formed by a substantial number of electrons (which is not the case for nuclear spins which can be effectively decoupled from the external world). All degrees of freedom interact with the environment thus causing the loss of quantum coherence. Whether this problem of decoherence can or cannot be satisfactorily solved is most likely to determine the future of JJ qubits.

The JJ qubit is made of superconducting islands separated by a Josephson junction; the scheme is depicted in Fig.2. In the scheme, 'SC' marks the
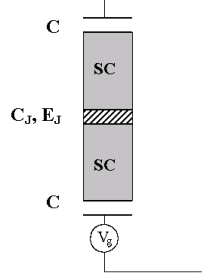

Fig. 2. Scheme for charge JJ qubit

superconducting islands and the hatched area is the Josephson junction with capacity C_J and Josephson coupling E_J. The superconductors are separated from the leads by capacitors C, which do not allow any tunneling, and these capacitors are biased by some controllable gate voltage V_g. Cooper pairs can tunnel through the Josephson junction thus changing the total charge of each island.

The charge JJ qubit is a two-level system which states are different by the charge of a single Cooper pair. The equilibrium number of Cooper pair in each island is controlled by the gate voltage. When it is tuned to be close to half integer $\sim n_0 + 1/2$, the states with n_0 and $n_0 + 1$ Cooper pairs (circled in Fig.3) can be arbitrarily close to each other in energy while the distance to other energy levels (crossed in Fig.3) is of the order of the charging energy that – in the temperature units - could be tens or even a hundred degrees of Kelvin which is much higher than typical experimental temperatures. We assume that the Josephson coupling energy is much smaller than the charging energy so that the states are really discriminated by charge. (In the opposite limit, a so called flux JJ qubit can be – very successfully – built). Thus we effectively separate all the charge states with $n < n_0$ or $n > n_0 + 1$ and thus have a two level system, whose states are made of a macroscopic number of electrons. In future we will be referring to these as states 'spin up' and 'spin down'.

More formally, the total energy of the system which consists of charging and Josephson contributions can be written as follows:

$$E = \frac{1}{2C_J + C} \left(2|e|n - \frac{CV_g}{2} \right)^2 - E_J \cos \Theta, \tag{14}$$

where Θ is the superconducting order-parameter phase shift between the islands. In properly chosen units, the pair of n and Θ are canonically conjugated
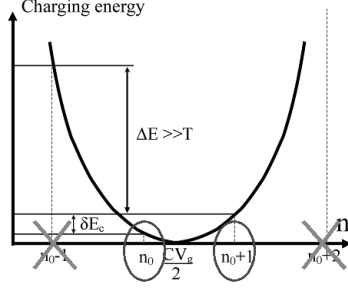
Fig. 3. Two charge states

coordinate and momentum since they generate correct Hamiltonian equations of motion. Differentiating with respect to momentum $\mathrm{d}n/\mathrm{d}t = \partial E/\partial \Theta = E_J \sin\Theta$ produces the correct equation for the Josephson current (in the units chosen E_J coincides with the critical current), and differentiation with respect to coordinate $\mathrm{d}\Theta/\mathrm{d}t = -\partial E/\partial n = (CV_g - 2n)/(2C_J + C) = V_J$ produces the correct value for the voltage drop V_J across the junction. The quantisation of (14) then gives:

$$\hat{H} = \frac{1}{2C_J + C}\left(\hat{n} - \frac{CV_g}{2}\right)^2 - E_J\cos\hat{\Theta}, \qquad \left[\hat{n}, \hat{\Theta}\right] = \mathrm{i}. \qquad (15)$$

After taking the projection of the Hamiltonian (15) onto two states of interest, in this 'spin up' and 'spin down' basis the charging part can be written as $(\delta E_c/2)\hat{\sigma}_z$, where δE_c is the charging energy difference between the two states:

$$\delta E_c(V_g) = \frac{2}{2C_J + C}\left(n_0 + \frac{1}{2} - \frac{CV_g}{2}\right). \qquad (16)$$

The commutator between $\hat{n}$ and $\hat{\Theta}$ dictates the commutation relations $[\hat{n}, e^{\pm \mathrm{i}\hat{\Theta}}] = \mp e^{\pm \mathrm{i}\hat{\Theta}}$ from which it immediately follows that in the 'spin up' and 'spin down' basis $\cos\hat{\Theta}$ is given by $\hat{\sigma}_x/2$. Summarizing the above we substitute the Hamiltonian (15) with its projection:

$$\hat{H} = \frac{\delta E_c(V_g)}{2}\,\hat{\sigma}_z - \frac{E_J}{2}\,\hat{\sigma}_x\,. \qquad (17)$$

As the result we have a controllable two level system or a qubit. The control is exercised by changing the gate voltage V_g on which the $\hat{\sigma}_z$ coefficient δE_c depends (16). If δE_c is maintained large $\delta E_c \gg E_J$, which is characteristic for charge JJ qubit, then the Josephson part of the Hamiltonian is irrelevant and evolution amounts to acquiring phase shift between 'spin up' and 'spin down' states in the initial mixture. On the contrary, tuning charging part to the degeneracy point $\delta E_c = 0$ stimulates the spin flip process. It can be

shown that the ability to switch for arbitrary time to the above two regimes is enough in order to provide all necessary one qubit quantum operations or quantum gates.

In building a quantum computer, one and two-qubit gates will be required. The details of how to build them are beyond the scope of these lectures and can be found in the comprehensive review [10] of Makhlin et. al. But what is crucial for any quantum computation is to maintain entanglement between the qubits. This will be undermined by inevitable decoherence. Therefore, understanding its mechanisms and studying how it sets in is crucial for future progress in this area.

4 Decoherence - Fluctuating Background Charges model

4.1 The model

The main problem with charge JJ qubits (as with any other solid state qubits) is that they lose quantum coherence too quickly due to unwanted, but unavoidable, coupling to the environment. Recent experiments [11–15]show that hundreds of elementary quantum operations can be achieved before coherence is destroyed. This is at least two orders of magnitude short [3] of a rough estimate of what is required for non-trivial quantum calculations. Thus the problem of decoherence is currently the major obstacle for the progress of qubits of this type, and requires a close theoretical examination.

Spin-boson models will not offer us any insight into how real physical parameters of the problem affect decoherence. To obtain this we need a physical model describing the real processes which decohere the qubit. It is widely believed [11, 12] that in charge JJ qubits the main contribution to decoherence comes from coupling of the qubit to some charge fluctuators present in the environment. The fluctuating background charges (FBC) model, suggested in this context in [4] and then also used in [5, 6, 7, 18], is an attempt to build a microscopic model for such a dominant channel of decoherence.

The schematic picture of how the qubit interacts with the FBC is shown in Fig.4. Impurities which contribute to decoherence sit on the substrate which the nanocircuit was grown on, close enough to a metallic lead to allow tunneling to and from the lead. Solid circles in Fig.4 are charged impurities and transparent circles are their image charges. These dipoles interact electrically with the qubit, which in turn behaves like a dipole, since one of the superconducting islands has some number of excessive Cooper pairs and the other one lacks the same number. The interaction depends on the number of such extra pairs and thus is different for the two charge states of the qubit, enforcing dependence of the coupling term on $\hat{\sigma}_z$. Although a static dipole-dipole interaction could only shift the qubit states without any loss of coherence, the tunneling between the impurities and the metallic lead makes charges on the impurities to fluctuate, effectively creating a random time-dependent field
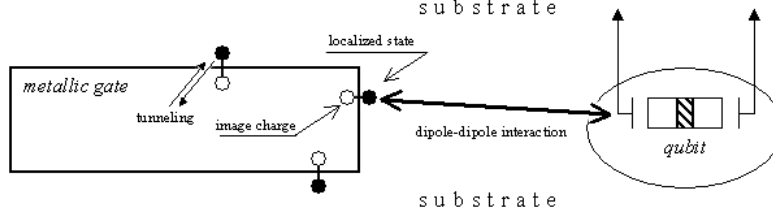
Fig. 4. Interaction between the qubit and fluctuating background charges

on the qubit. This random field causes decoherence. This is similar to the generic case considered in Section 2: the time-dependent electric field coupled to σ_z plays the role of the random 'magnetic field' B_z in Eq. (8). In the following section, we will show that within the Fermi golden rule approximation (valid for a weak coupling between the qubit and the FBC), both decoherence and relaxation can be calculated in a way similar to that schematically developed in Section 2, with an additional advantage of calculating the noise power-spectrum within a fully microscopical model. In this section, we restrict considerations to the longitudinal model of pure decoherence. Its advantage is that one can go well beyond the Fermi golden rule, and calculate the decoherence rate (but not the relaxation!) non-perturbatively and within a fully quantum description valid for any temperature, including $T \to 0$ (in which limit there is no decoherence in the absence of relaxation).

The Hamiltonian corresponding to the described model can be written as

$$\hat{H} = \frac{\delta E_c}{2}\,\hat{\sigma}_z - \frac{E_J}{2}\,\hat{\sigma}_x + \hat{\sigma}_z \hat{V} + \hat{H}_{\mathrm{B}}; \qquad \hat{V} = \frac{1}{2}\sum_i v_i\,\hat{d}_i^\dagger \hat{d}_i \;;$$

$$\hat{H}_{\mathrm{B}} = \sum_i \varepsilon_i^0 \hat{d}_i^\dagger \hat{d}_i \; + \sum_{i,\mathbf{k}}\left[t_{\mathbf{k}i}\hat{c}_{\mathbf{k}}^\dagger \hat{d}_i \; + \; \mathrm{h.c}\right] + \sum_{\mathbf{k}}\varepsilon_{\mathbf{k}}\hat{c}_{\mathbf{k}}^\dagger \hat{c}_{\mathbf{k}}. \qquad (18)$$

Here $\hat{d}_i$, $\hat{d}_i^\dagger$ are the operators of annihilation and creation of an electron on the i-th impurity; $\hat{c}_{\mathbf{k}}$, $\hat{c}_{\mathbf{k}}^\dagger$ are the operators of the conduction electrons in the metal; $t_{\mathbf{k}i}$ are the hybridisation amplitudes; ε_i^0 is the energy of the localised state on the i-th impurity; $\varepsilon_{\mathbf{k}}$ are the energies of the conducting electrons; v_i is the coupling strength between the qubit and the ith impurity.

The charge JJ qubit corresponds to $\delta E_c \gg E_J$, which is always the case for the small enough capacities (i.e. small superconducting islands and the JJ junction in Fig. 2. A non-trivial circuit is supposed to consist of many qubits, and most of the time each particular qubit is in an idle regime for which the condition above is fulfilled. During relatively short times necessary for operations involving spin-flips the longitudinal model, $E_J = 0$, is not

appropriate. However, if there is any hope for a working qubit, the onset of decoherence should only happen in the idle regime.

Apart from temperature, there are three other parameters of dimensions of energy for each fluctuator: the coupling strength v_i, tunneling rate γ_i ($\gamma_i = 2\pi \sum_{\mathbf{k}} |t_{\mathbf{k}i}|^2 \delta(\omega - \varepsilon_{\mathbf{k}})$), and fluctuator energy ε_i (note that the bare energy ε_i^0 is renormalised by hybridisation). All three parameters are broadly distributed, and temperature can be considered 'low' for some of them and 'high' for others. In the Section 5 we will show that these two regimes are defined as follows:

$$
\begin{cases}
T \ll \min \left| \varepsilon_i \pm \frac{1}{2}\sqrt{v_i^2 - \gamma_i^2} \right| \quad \text{or} \quad T \ll \gamma_i \qquad \text{low-T regime} \\[3mm]
T \gg \max \left| \varepsilon_i \pm \frac{1}{2}\sqrt{v_i^2 - \gamma_i^2} \right| \text{ and } \quad T \gg \gamma_i \qquad \text{high-T regime}
\end{cases}
\tag{19}
$$

In the high-temperature regime, the decoherence rate can be calculated classically [4, 5] which gives for one fluctuators (omitting the index i)

$$
\Gamma_2 = \frac{\gamma}{2} \left[1 - \Re\sqrt{1 - \frac{v^2}{\gamma^2}} \right] =
\begin{cases}
\gamma/2\,, \quad v > \gamma \\[3mm]
v^2/4\gamma\,, \, v \ll \gamma
\end{cases}
\tag{20}
$$

The high temperature treatment of the model would be justified if the high energy impurities, $|\varepsilon_i| \gtrsim T$, were frozen. However, the same hybridisation γ which makes impurity charges to fluctuate, broadens their energy positions. Such a broadening creates a Lorentzian tail which is, of course, power-law suppressed but nevertheless allows for a contribution from the energetically remote impurities. Moreover, even impurities with $|\varepsilon_i| \ll T$ may not satisfy the high-T inequality (19) and contribute in a non-classical way. We will present below some arguments that the impurities most relevant for decoherence are likely to to be in the low-temperature regime.

4.2 Why low temperature?

Let us first illustrate why the hybridisation leads to the Lorentzian tail. To simplify notation, we will be considering a single impurity. The quadratic Hamiltonian of the bath $\hat{H}_{\mathrm{B}}$ can be diagonalised by means of some linear transformation [19], after which it becomes $\hat{H}_{\mathrm{B}} = \sum_n \epsilon_n \hat{\alpha}_n^\dagger \hat{\alpha}_n$. The interaction part $\hat{V}$ gets transformed into a sum over all exact states: $\hat{V} = (v/2) \sum_{n,m} u_n^* u_m \hat{\alpha}_n^\dagger \hat{\alpha}_m$, where coefficients u_n are related to the density of states (DoS) $\nu_\varepsilon(\omega)$ on the impurity broadened by hybridisation with the conduction band: $|u_n|^2 = \nu_\varepsilon(\epsilon_n)\delta$; here δ is the level spacing in the conduction band, and the DoS is given by the Lorentzian

$$
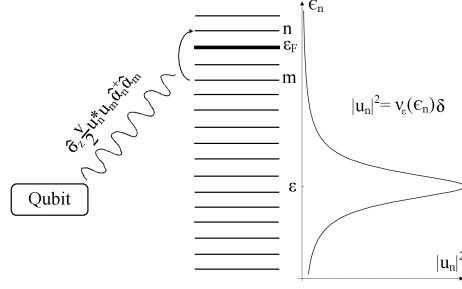\nu_\varepsilon(\omega) = \frac{1}{\pi} \frac{\gamma/2}{(\omega - \varepsilon)^2 + \gamma^2/4}\,.
\tag{21}
$$

Fig. 5. Qubit is coupled to the transitions between all exact states of the bath Hamiltonian $\hat{H}_{\mathrm{B}}$, with weight being proportional to $u_n^* u_m$. Coefficients u_n^*, u_m are governed by the Lorentzian $|u_n|^2 = \nu_\varepsilon(\epsilon_n)\delta$.

In this notation, low temperature manifests itself in smallness of the interaction term $\hat{V}$, to which only n and m in the vicinity of the Fermi level will effectively contribute (see Fig.5). Since the smallness of u coefficients is controlled by the Lorentzian (21)(rather than distribution function), the effect of such a high energy impurity can only be power law suppressed.

The second observation concerns very stringent geometrical restrictions on where an 'effective' impurity can be and a broad distribution of energies of impurities. In order to allow tunneling to and from the impurity, it should not be too far away from the metallic gate, which implies that the total volume available for 'effective' impurities cannot exceed $1\mu m \times (10\lambda_F)^2$, where $1\mu m$ is a characteristic size of a metallic gate and λ_F is the Fermi wavelength in the metal. If we are hoping to find at least one low energy $|\varepsilon_i| < T$ impurity in this volume, the total number of impurities there should be of order of D/T, where D is the width of the distribution function of energies. For temperature which varies in experiments between $30mK$ and $50mK$, and for D having a typical chemical value of $1eV$ the above ratio is of order of 10^5. Having that many impurities in a volume which in total accommodates $\sim 10^6$ atoms is completely unrealistic.

So, the contribution of high energy impurities is suppressed but not strongly enough in order to exclude them from consideration, and low energy impurities effectively do not exist. If for a particular sample there happened to be one, this sample will exhibit orders of magnitude stronger decoherence, and should better be discarded.

The condition $|\varepsilon_i| \gg T$ enforces low temperature regime which requires a full quantum mechanical treatment. Such a treatment, valid at any temperature, will be offered in the next Section.

5 Exact solution for FBC model at arbitrary temperature

5.1 Calculations

To calculate the decoherence rate we will need to know how the off-diagonal elements of the reduced density matrix of the qubit decay with time. The dynamics of the full density matrix of the whole system qubit + bath is given by the Heisenberg equation of motion:

$$\frac{\partial \hat{\rho}(t)}{\partial t} = -\mathrm{i}\left[\hat{H}, \hat{\rho}(t)\right],\tag{22}$$

where $\hat{H}$ is the Hamiltonian given by the Eq. (18) with Josephson energy being taken equal to zero. Since in the longitudinal ($E_J = 0$) model the interaction term commutes with the qubit Hamiltonian, one can trace out the bath degrees of freedom thus yielding the following result for the reduced density matrix of the qubit:

$$\hat{\rho}^{(q)}(t) = \begin{pmatrix} \rho_{11}^{(q)}(0) & \rho_{12}^{(q)}(0)\,e^{-\mathrm{i}\delta E_c t}D(t) \\ \rho_{21}^{(q)}(0)\,e^{\mathrm{i}\delta E_c t}D^*(t) & \rho_{22}^{(q)}(0) \end{pmatrix},\tag{23}$$

where the standard separable initial condition for the full density matrix, $\hat{\rho}(0) = \hat{\rho}^{(q)}(0) \otimes \hat{\rho}_B$; $\hat{\rho}_B = \mathrm{e}^{-\beta \hat{H}_\mathrm{B}}/\mathrm{Tr}\,\mathrm{e}^{-\beta \hat{H}_\mathrm{B}}$, was assumed. The diagonal elements of the reduced density matrix do not evolve since there are no spin flip processes present, and the dynamics of the off-diagonal elements is governed by the decoherence function $D(t)$:

$$D(t) = \left\langle e^{\mathrm{i}(\hat{H}_\mathrm{B}+\hat{V})t}\mathrm{e}^{-\mathrm{i}(\hat{H}_\mathrm{B}-\hat{V})t}\right\rangle,\tag{24}$$

where averaging should be performed with the bath Hamiltonian $\hat{H}_\mathrm{B}$. At long times t the decoherence function must decay exponentially, $D(t) \sim \mathrm{e}^{-\Gamma_2 t}$, so that the decoherence rate Γ_2 is defined as

$$\Gamma_2 = -\Re\mathrm{e}\lim_{t\to\infty} t^{-1}\ln D(t),\tag{25}$$

in the agreement with Eq. (9).

The average in Eq. (24) can be represented as the following functional integral with the Grassmann fields ξ and η defined on the Keldysh contour:

$$D(t) = Z^{-1}\int \mathcal{D}\xi^* \mathcal{D}\xi \mathcal{D}\eta^* \mathcal{D}\eta\, e^{\mathrm{i}S_0[\xi]}\, e^{\mathrm{i}S_0[\eta]}\, e^{\frac{\mathrm{i}}{2}\int_{c_K}\sum_i v_i(t')\xi_i^*(t')\xi_i(t')\mathrm{d}t'} \times$$
$$\times\, e^{-\mathrm{i}\int_{c_K}\sum_{\mathbf{k},i}\left[t_{\mathbf{k}i}\eta_{\mathbf{k}}^*(t')\xi_i(t')+t_{\mathbf{k}i}^*\xi_i^*(t')\eta_{\mathbf{k}}(t')\right]\mathrm{d}t'}.\tag{26}$$

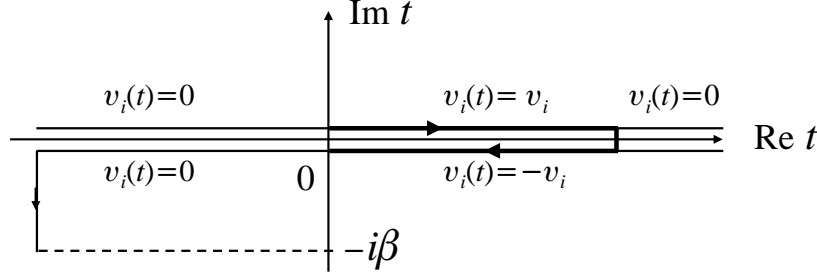**Fig. 6.** Dependence of $v_i(t)$ on time along the Keldysh contour

Here Z is the same functional integral but with $v_i(t') \equiv 0$, the fields ξ_i, ξ_i^* correspond to the localised state on the i-th impurity, $\eta_{\mathbf{k}}$, $\eta_{\mathbf{k}}^*$ to the conduction electrons, the impurity $S_0[\xi]$ and free electrons $S_0[\eta]$ actions are given by:

$$S_0[\xi] = \int_{c_K} \sum_i \xi_i^*(t')(\mathrm{i}\partial_{t'} - \varepsilon_i^0)\xi_i(t')\mathrm{d}t'$$

$$S_0[\eta] = \int_{c_K} \sum_{\mathbf{k}} \eta_{\mathbf{k}}^*(t')(\mathrm{i}\partial_{t'} - \varepsilon_{\mathbf{k}})\eta_{\mathbf{k}}(t')\mathrm{d}t' \,, \tag{27}$$

and the Keldysh time dependent coupling $v_i(t')$ is zero everywhere on the contour apart from the interval $(0, t)$ where on the upper branch it takes the value of v_i, and on the lower branch it is equal to $-v_i$ (see Fig.6). Since the action $S_0[\eta]$ is quadratic and the hybridisation term is linear in η fields, it is straightforward to integrate out the conduction electrons:

$$D(t) = Z_0^{-1} \int \mathcal{D}\xi^* \mathcal{D}\xi \, e^{\mathrm{i}S_0[\xi]} \, e^{-\mathrm{i}\iint_{c_K} \sum_{ij} \xi_i^*(t_1)\Sigma_{ij}(t_1,t_2)\xi_j(t_2)\mathrm{d}t_1\mathrm{d}t_2}$$

$$e^{\frac{\mathrm{i}}{2} \int_{c_K} \sum_i v_i(t_1)\xi_i^*(t_1)\xi_i(t_1)\mathrm{d}t_1} \tag{28}$$

Again, here Z is the same functional integral but with $v_i(t') \equiv 0$. All the information about the conduction electrons is now encoded in the self-energy matrix which is defined on the contour:

$$\Sigma_{ij}(t_1, t_2) = \sum_{\mathbf{k}} t_{\mathbf{k}i}^* t_{\mathbf{k}j} g_{\mathbf{k}}(t_1, t_2) \,, \qquad t_1, t_2 \in c_K \tag{29}$$

with $g_{\mathbf{k}}(t_1, t_2)$ being the Green function of free electrons. The full action in (28) is quadratic and therefore the corresponding functional integral can be

written in a standard symbolic trace-log notation:

$$D(t) = e^{\operatorname{Tr} \ln\left[\hat{1}+\hat{G}\hat{U}\right]}, \tag{30}$$

where both $\hat{G}$ and $\hat{U}$ are matrices in the space of impurity indices, and both depend on two times along the Keldysh contour. The symbol Tr here stands for trace with respect to the impurity indices and for integration along the Keldysh contour over all the times involved. The Green function $\hat{G}$ obeys the following integro-differential equation:

$$\int_{c_K} dt' \sum_m \left[\delta_{im}\delta(t_1,t')\left(\mathrm{i}\frac{\partial}{\partial t'} - \varepsilon_m^0\right) - \Sigma_{im}(t_1,t')\right] G_{mj}(t',t_2) = \delta_{ij}\delta(t_1,t_2), \tag{31}$$

with δ-function $\delta(t_1,t_2)$ being defined on the contour. The impurity matrix $\hat{U}$ is made out of the time-dependent coupling $v_i(t')$:

$$U_{ij}(t_1,t_2) = \delta_{ij}\delta(t_1,t_2)\frac{v_i(t_2)}{2}. \tag{32}$$

Being written explicitly, the symbolic expression in (30) becomes

$$D(t) = e^{-\sum_{n=1}^{\infty}\frac{(-1)^n}{n}\ \operatorname{tr}\ \underset{\substack{c_K \\ 2n\ \text{integrals}}}{\int\cdots\int}\ dt_1 dt_1'...dt_n dt_n' \hat{G}(t_1,t_1')\hat{U}(t_1',t_2)...\hat{G}(t_n,t_n')\hat{U}(t_n',t_1)} \tag{33}$$

where tr stands for a trace over impurity indices only.

Since the matrix $\hat{U}(t_1,t_2)$ as function of its both times is non-vanishing only between 0 and t, all the contour integrals in (33) can be converted into ordinary integrals from 0 to t by introducing the Keldysh structure for both matrices $\hat{G}$ and $\hat{U}$. Both arguments of $\hat{G}(t_1,t_2)$ can either be on the upper or on the lower branch of the Keldysh contour leaving four choices which generate the following Keldysh structure:

$$G_{ij}(t_1,t_2)_{t_{1,2}\in c_K} \mapsto \check{\mathcal{G}}_{ij}(t_1-t_2)_{t_{1,2}\in(-\infty,+\infty)} = \begin{pmatrix} \mathcal{G}_{ij}(t_1-t_2) & \mathcal{G}_{ij}^{<}(t_1-t_2) \\ \mathcal{G}_{ij}^{>}(t_1-t_2) & \widetilde{\mathcal{G}}_{ij}(t_1-t_2) \end{pmatrix} \tag{34}$$

where $\mathcal{G}_{ij}(t_1-t_2)$ and $\widetilde{\mathcal{G}}_{ij}(t_1-t_2)$ are the time-ordered and anti-time-ordered Green functions. Using the Keldysh structure for the $\hat{U}$-matrix,

$$U_{ij}(t_1,t_2)_{t_{1,2}\in c_K} \mapsto \tfrac{1}{2}\delta_{ij}\,\hat{\sigma}_z\,\delta(t_1-t_2)\,v_i(t_2)_{t_{1,2}\in(-\infty,+\infty)},$$

and the general rule,

$$\int_{c_K} A(t_1,t')B(t',t_2)dt'\bigg|_{t_{1,2}\in c_K} \mapsto \int_{-\infty}^{+\infty} \check{A}(t_1,t')\hat{\sigma}_z\check{B}(t',t_2)dt'\bigg|_{t_{1,2}\in(-\infty,+\infty)},$$

we rewrite the expression (33) for the decoherence function as follows:

$$D(t) = e^{-\sum\limits_{n=1}^{\infty} \frac{(-1)^n}{n2^n} \operatorname{Tr} \int\limits_0^t ... \int\limits_0^t dt_1 dt_2 ... dt_n \breve{\mathcal{G}}(t_1-t_2)(\hat{v}\otimes\hat{1})\breve{\mathcal{G}}(t_2-t_3)(\hat{v}\otimes\hat{1})...\breve{\mathcal{G}}(t_n-t_1)(\hat{v}\otimes\hat{1})}$$

(35)

Now the symbol Tr stands for the trace over both impurity and Keldysh matrix indices, while $(\hat{v}\otimes\hat{1})$ denotes the matrix with elements v_i on the main diagonal in the impurity space and which is the unity matrix in the Keldysh space.

It is convenient to do a standard rotation [20] in Keldysh space:

$$\hat{\mathcal{G}}_{ij} = \hat{L}\hat{\sigma}_z\breve{\mathcal{G}}_{ij}\hat{L}^\dagger; \qquad \hat{L} = \frac{1}{\sqrt{2}}(\hat{1} - \mathrm{i}\hat{\sigma}_y),$$

(36)

which converts the four-element matrix in (34) into the three-element one of retarded, advanced and Keldysh Green functions:

$$\hat{\mathcal{G}}_{ij} = \begin{pmatrix} G_{ij}^R & G_{ij}^K \\ 0 & G_{ij}^A \end{pmatrix}$$

(37)

In the rotated basis the expression (35) for the decoherence function becomes:

$$D(t) = e^{-\sum\limits_{n=1}^{\infty} \frac{(-1)^n}{n2^n} \operatorname{Tr} \int\limits_0^t ... \int\limits_0^t dt_1 dt_2 ... dt_n (\hat{v}\otimes\hat{\sigma}_x)\hat{\mathcal{G}}(t_1-t_2)(\hat{v}\otimes\hat{\sigma}_x)\hat{\mathcal{G}}(t_2-t_3)...(\hat{v}\otimes\hat{\sigma}_x)\hat{\mathcal{G}}(t_n-t_1)}$$

(38)

Since due to the time translation invariance each $\hat{G}$ depends only on the difference of its time arguments, the nth order integrand depends on $n-1$ differences in times, while the integration over the last time variable produces the overall factor of t. The region of integration becomes, at arbitrary time, quite complicated. However, when time t is much bigger than the characteristic time on which $\hat{\mathcal{G}}(\tau)$ function decays (which is true if $t \gg \gamma_i^{-1}, T^{-1}$), all the integrals over the time differences can be extended to the entire axis. Then the integral has a convolution structure in time and, performing a Fourier transform and a straightforward summation that restores the logarithm, it finally reduces to

$$D(t) = e^{-t \int\limits_{-\infty}^{+\infty} \frac{d\omega}{2\pi} \operatorname{Tr} \ln\left[\hat{1}+\frac{1}{2}(\hat{v}\otimes\hat{\sigma}_x)\hat{\mathcal{G}}(\omega)\right]}.$$

(39)

Using the definition of decoherence rate (25) and calculating trace in the Keldysh space explicitly we have:

$$\Gamma_2 = -\Re e \int\limits_{-\infty}^{+\infty} \frac{d\omega}{2\pi} \operatorname{tr} \ln\left[\hat{1} + \frac{\hat{v}}{2}\hat{G}^K(\omega) - \frac{\hat{v}}{2}\hat{G}^R(\omega)\frac{\hat{v}}{2}\hat{G}^A(\omega)\right],$$

(40)

where tr refers only to the impurity matrix indices.

It should be stressed that the analytical structure of the expression in the r.h.s. of Eq. (40) ensures that there is no decoherence at zero temperature. Indeed, using the standard relation [20] between the components of Keldysh Green functions at equilibrium, $\hat{G}^K(\omega) = \tanh(\beta\omega/2)[\hat{G}^R(\omega) - \hat{G}^A(\omega)]$, which at $T = 0$ reduces to $\hat{G}^K(\omega) = \mathrm{sgn}(\omega)[\hat{G}^R(\omega) - \hat{G}^A(\omega)]$, we have:

$$\Gamma_2(T = 0) = -\Re e \int\limits_{-\infty}^{+\infty} \frac{\mathrm{d}\omega}{2\pi} \, \mathrm{tr}\ln\left[\left(\hat{1} + \frac{\hat{v}}{2}\hat{G}^R(\omega)\right)\left(\hat{1} - \frac{\hat{v}}{2}\hat{G}^A(\omega)\right)\right] . \quad (41)$$

Separating the retarded and advanced parts in the expression above, and then expanding the logarithm in both of them, we see that starting from the second order all the integrals are convergent at $\omega \to \infty$ and therefore equal to zero since the retarded (advanced) Green function is analytic in the upper (lower) half plane. Combining the first order contributions from both parts we see that it is purely imaginary and therefore also vanishes.

Assuming that the impurity states are well localised, the tunneling amplitudes $t_{\mathbf{k}i}$ can be written as $t_{\mathbf{k}i} = t_i \mathrm{Vol}^{-1/2} e^{\mathrm{i}\mathbf{k}\mathbf{r}_i}$, where $\mathbf{r}_i$ is the position of the i-th impurity. This in turn means that the self energy matrix (29) has the following representation:

$$\hat{\Sigma}_{ij}(t_1 - t_2) = t_i^* t_j \hat{g}(t_1 - t_2; \mathbf{r}_j - \mathbf{r}_i) . \quad (42)$$

Since the characteristic distance l between the impurities is much bigger than the Fermi wavelength, $l \gg \lambda_F$, all the off-diagonal elements of the self energy matrix will be averaged out while diagonal can be represented as

$$\Sigma_{ii}^{A/R}(\omega) = \left[\sum_{\mathbf{k}} \frac{|t_{\mathbf{k}i}|^2}{\omega - \varepsilon_{\mathbf{k}}} \pm \mathrm{i}\pi\sum_{\mathbf{k}} |t_{\mathbf{k}i}|^2 \delta(\omega - \varepsilon_{\mathbf{k}})\right] = \left[\frac{\alpha_i(\omega)}{2} \pm \mathrm{i}\frac{\gamma_i(\omega)}{2}\right] . \quad (43)$$

This allows one to solve (the Keldysh rotated analogue of) Eq. (31):

$$G_{ij}^{A/R}(\omega) = \frac{\delta_{ij}}{\omega - \varepsilon_i^0 - \Sigma_{ii}^{A/R}(\omega)} = \frac{\delta_{ij}}{\omega - \varepsilon_i \mp \mathrm{i}\gamma_i/2} , \quad (44)$$

where both the real and imaginary parts of the self energy matrix were assumed ω-independent, and the real part was absorbed by renormalisation of the energy levels $\varepsilon_i = \varepsilon_i^0 + \alpha_i/2$. In such a diagonal approximation for the self-energy, the contributions from all the impurities are independent and the total decoherence rate is given by their sum. Substituting Eq. (44) for the Green functions into Eq. (40), subtracting (to improve the integral convergency) the identically zero expression (41) for Γ_0 and taking the real part of the resulting expression, we obtain the following contribution of a single impurity at energy $\varepsilon_j \equiv \varepsilon$ to the decoherence rate:

$$\Gamma_2(T) = -\int\limits_{-\infty}^{+\infty} \frac{d\omega}{4\pi} \ln\left[1 - \frac{v^2\gamma^2\cosh^{-2}(\omega/2T)}{v^2\gamma^2 + 4\left[(\omega-\varepsilon)^2 + \gamma^2/4 - v^2/4\right]^2}\right].$$ (45)

5.2 Discussion of the results

It is convenient to introduce an auxiliary 'spectral function' $\Lambda(\omega)$,

$$\Lambda(\omega) = \frac{1}{1 + 4(\omega-\varepsilon_+)^2(\omega-\varepsilon_-)^2/v^2\gamma^2}, \qquad \varepsilon_\pm = \varepsilon \pm \frac{1}{2}\sqrt{v^2-\gamma^2}, \quad (46)$$

thus rewriting Eq. (45) as follows:

$$\Gamma_2(T) = -\int\limits_{-\infty}^{+\infty} \frac{d\omega}{4\pi} \ln\left[1 - \Lambda(\omega)\cosh^{-2}\frac{\omega}{2T}\right].$$ (47)

Behaviour of $\Lambda(\omega)$ is qualitatively different depending on whether $g \equiv v/\gamma < 1$ or $g > 1$. In the former case $\Lambda(\omega)$ is peaked at $\omega = \varepsilon$, while in the latter the peak splits into two Lorentzians which are centered at $\omega = \varepsilon_\pm$ and travel in different directions away from the $\omega = \varepsilon$ point as v increases. This signals a qualitative change between the weak coupling ($g \ll 1$) and the strong coupling ($g \gg 1$) regimes.

The decoherence rate is determined by the overlap of the temperature function, $\cosh^{-2}(\omega/2T)$, and $\Lambda(\omega)$ in (47). The former is centered at $\omega = 0$ and exponentially decays for $|\omega| > T$, while the latter has the power-law decay away from the above described peaks. If the temperature function is wide and the Lorentzian peaks are sitting inside T, the overlap is solely controlled by $\Lambda(\omega)$ as if the temperature function was equal to 1 everywhere. In the opposite case when the temperature function is narrow either with respect to the distance to the Λ-function peaks or to their width, the overlap is controlled by $\cosh^{-2}(\omega/2T)$ and $\Lambda(\omega)$ can be replaced by $\Lambda(\omega = 0)$. We will be calling these two cases high-temperature ($T \gg \max|\varepsilon_\pm|, \gamma$) and low-temperature ($T \ll \min|\varepsilon_\pm|$ or $T \ll \gamma$) regimes correspondingly.

In the high-temperature regime, $T \gg \max|\varepsilon_\pm|, \gamma$, the decoherence rate Γ_2 saturates [4, 5] at ε-independent value:

$$\Gamma_2^{(\mathrm{high})} = -\int\limits_{-\infty}^{+\infty} \frac{d\omega}{4\pi} \ln\left[1 - \Lambda(\omega)\right] = \frac{\gamma}{2}\left[1 - \Re\sqrt{1-g^2}\right].$$ (48)

In the low-T regime, when either $T \ll \min|\varepsilon_\pm|$ or $T \ll \gamma$, the decoherence rate becomes linear in temperature:

$$\Gamma_2^{(\text{low})}(T) = -\int\limits_{-\infty}^{+\infty} \frac{d\omega}{4\pi} \ln\left[1 - \Lambda(\omega = 0)\cosh^{-2}\frac{\omega}{2T}\right]$$

$$= \frac{T}{\pi}\arctan^2\left(\frac{2g}{4\varepsilon^2/\gamma^2 - g^2 + 1}\right). \tag{49}$$

When both the coupling strength v and energy ε are smaller than the tunneling rate γ, the regime change occurs in the vicinity of $T \sim \gamma$ point (the upper curve on the insert in Fig.7). If γ is smaller than either of the other two parameters: $\gamma \ll A = \max\{\varepsilon, v/2\}$, then the high- and low-temperature asymptotes parametrically mismatch. In this case there is a crossover between the two regimes which is exponentially fast and occurs in the logarithmically narrow interval of temperatures:

$$\Gamma_2^{(\text{x-over})}(T) \sim \Gamma_2^{(\text{high})}e^{-A/T}, \qquad \frac{A}{\ln A/\gamma} \lesssim T \lesssim A. \tag{50}$$

The temperature dependence of the decoherence rate is shown in Fig.7 for the case of different couplings and fluctuator energies. We should stress that
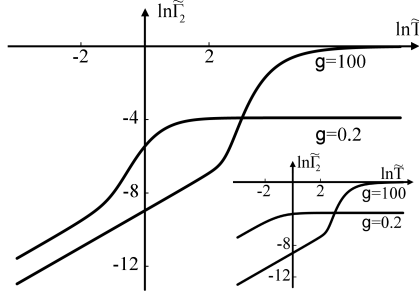

Fig. 7. Dependence of the decoherence rate on temperature, Eq.(47), for strong and weak coupling. The main picture shows a fluctuator with $\nu_\varepsilon(\omega)$ centered at $\tilde{\varepsilon} = 3$, the insert shows $\tilde{\varepsilon} = 0$. $\tilde{T}, \tilde{\Gamma}_2, \tilde{\varepsilon}$ are measured in units of $\gamma/2$.

although a linear in T behaviour similar to that in the Eq.(49) would also follow from the spin-boson models with the ohmic spectral function, as briefly described in Section 2, only a full quantum mechanical treatment can result in a non-trivial T dependence depicted in Fig.7.

Let us also stress that, although that at high temperatures decoherence is always stronger for a strongly coupled fluctuator, this does not have to be the case as temperature is lowered, since in the crossover region the $g \gg 1$ fluctuators undergo stronger suppression than their $g \ll 1$ counterparts. Such a non-monotonic dependence of the decoherence rate Γ_2 on the coupling strength v outside the classical region of high T deserves special attention.

When we start with a small value of v, $v < \gamma$, the peak of $\Lambda(\omega)$ grows as v increases which leads to higher decoherence rate Γ_2. This proceeds on until the $v = \gamma$ point is reached when the peak stops growing but splits into two instead. One of those peaks then starts moving towards the origin which increases the overlap between the temperature function and $\Lambda(\omega)$, so Γ_2 keeps on growing. The maximum possible overlap is achieved when the incoming Lorentzian is centered at $\omega = 0$ which happens at the $v = \sqrt{4\varepsilon^2 + \gamma^2}$ point. If the coupling strength is increased beyond this point, the peak of $\Lambda(\omega)$ becomes de-tuned from the peak of the temperature function and the decoherence rate goes down. Since $\Lambda(\omega)$ plays the role of a spectral function, the positions of its maxima $\varepsilon_\pm$ give us the energies of charge states of the system. Pushing them away from the Fermi level leads to freezing them out so that the impurity is no longer a fluctuator and thus does not contribute to the decoherence rate. Note that such a strong coupling is still not a good news for the qubit operation as the qubit and the impurity form together a four-level system which, although remains coherent, does not operate as intended.

The above described behaviour of the decoherence rate as a function of coupling strength is depicted in Fig.8. Note that the maximum of Γ_2 has a cusp which is not smeared by temperature (but would be smeared by including the σ_x part into the Hamiltonian): Only at a rater high temperature ($\tilde{T} \sim 100$)
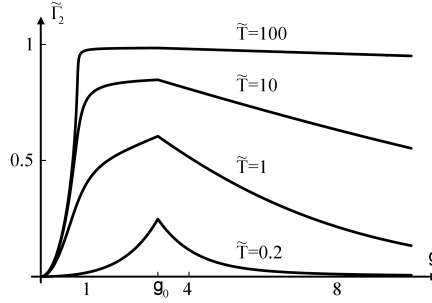

Fig. 8. Non-monotonic dependence of the decoherence rate on the coupling strength at different temperatures for $\tilde{\varepsilon} = 3$; here $g_0 = \sqrt{\tilde{\varepsilon}^2 + 1}$.

the decoherence rate practically saturates at its classical limit $\Gamma_2^{\text{(high)}} = \gamma/2$.

6 Relaxation in the FBC model

Apart from decoherence, coupling of a qubit to the environment also leads to relaxation processes, i.e. to a decay of diagonal elements of the density matrix (23), as outlined in Section 2. In the model under consideration, Eq. (18), the presence of the $\hat{\sigma}_x$-part inevitably induces relaxation. Such a relaxation would also destroy coherence but the relaxation rate Γ_1 is typically smaller than the

decoherence rate Γ_2 and therefore the time available for quantum operations is going to be determined by the latter. Experiments on the relaxation rate are of special interest as they can provide valuable information about the degrees of freedom in the environment to which qubit is coupled.

It is convenient to diagonalize the qubit part of the Hamiltonian (18), transforming simultaneously the interaction part $\hat{\sigma}_z$ into a sum of $\hat{\tau}_z$ and $\hat{\tau}_x$ terms - the Pauli matrices in the new basis:

$$\hat{H} = \frac{\Delta E}{2}\,\hat{\tau}_z + (\cos\Theta\,\hat{\tau}_z + \sin\Theta\,\hat{\tau}_x)\,\hat{V} + \hat{H}_{\mathrm{B}}\,; \quad \text{where}$$

$$\Delta E = \sqrt{(\delta E_c)^2 + E_J^2}\,, \quad \cos\Theta = \frac{\delta E_c}{\Delta E}\,, \quad \sin\Theta = \frac{E_J}{\Delta E}\,. \tag{51}$$

As it is well known [17], in Born-Markov rotating-wave approximation the decoherence rate Γ_1 is given by:

$$\Gamma_1 = \sin^2\Theta\,S(\Delta E)\,, \qquad S(\Omega) = \left\langle \left\{ \hat{V}(t) - \langle\hat{V}\rangle, \hat{V}(t') - \langle\hat{V}\rangle \right\} \right\rangle_\Omega\,, \tag{52}$$

where $S(\Omega)$ is the spectral density of noise. (The appropriate derivation is outlined in Section 2). The symbol $\langle\ldots\rangle_\Omega$ denotes the Fourier transform of the bath-averaged expression with respect to $t - t'$ at the frequency Ω.

In the experiment of Astafiev et al [8] the authors determined the spectral density of noise in a wide window of frequencies, by changing ΔE and measuring the relaxation rate. The experimental data for $S(\Omega)$ is presented in Fig.9. Although the data points are somewhat scattered, the authors nevertheless
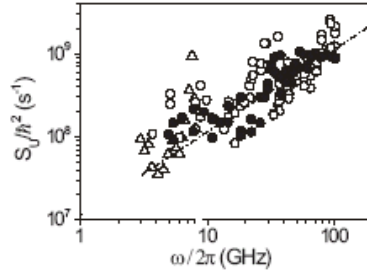

Fig. 9. The experimental data by Astafiev et al [8]: the noise spectral density S deduced from measurements of Γ_1; open and closed symbols correspond to different samples while circles and triangles – to different measurement regimes; $T \approx 50\mathrm{mK}$.

claim that they observed a linear behaviour of spectral density of noise with peaks at 7 and 23GHz.

Below we will demonstrate that qualitatively the same behaviour is expected from $S(\Omega)$ in the FBC model at low temperatures. A contribution to the spectral density of noise from one impurity is given by

$$S(\Omega) = \frac{v^2}{4} \left\langle \left\{ \hat{d}^\dagger(t)\hat{d}(t) - \langle \hat{d}^\dagger \hat{d} \rangle, \, \hat{d}^\dagger(t')\hat{d}(t') - \langle \hat{d}^\dagger \hat{d} \rangle \right\} \right\rangle_\Omega =$$

$$= \frac{\pi v^2}{2} \coth \frac{\Omega}{2T} \int\limits_{-\infty}^{+\infty} \mathrm{d}\omega \, \nu_\varepsilon(\omega)\nu_\varepsilon(\omega + \Omega) \left[n_F(\omega) - n_F(\omega + \Omega) \right], \quad (53)$$

where the density of states $\nu_\varepsilon(\omega)$ is given by (21), and $n_F(\omega)$ is the Fermi distribution function.

The frequencies accessed in the experiment [8] are in the window $T \ll \Omega < 100T$. Getting back to the rough estimates for the probability of having an effective impurity with energy smaller than temperature (the end of Section 4), we see that even a scenario with $|\varepsilon_i| \gg 100T$ for all effective impurities is quite likely. If this is the case then the condition $T \ll \Omega \ll |\varepsilon|$ holds and it is clear that the spectral density of noise $S(\Omega)$ exhibits linear behaviour at such frequencies. As the thermal factor is practically equal to 1 within the range $-\Omega < \omega < 0$ and zero otherwise, the smearing of this step is of the order of temperature. Far to the right (assuming ε to be positive) we have two peaks in DoS at $\varepsilon - \Omega$ and ε. The main contribution to the integral (53) is coming from the tails of ν_ε at the interval $-\Omega < \omega < 0$, rather than from the thermal function tail in the vicinity of DoS peaks which is exponentially suppressed. The latter contribution would only win if γ itself was exponentially small, but the corresponding impurity is obviously non-effective. If γ is not too small, we find

$$S(\Omega) = \frac{\pi v^2}{2} \nu_\varepsilon^2(0)\Omega \qquad T \ll \Omega \ll \varepsilon. \qquad (54)$$

The summation of contributions (54) coming from all the effective impurities produces a linear in Ω function, which can be a possible explanation for a linear (but very noisy) trend in $S(\Omega)$ observed in [8].

Humps in Fig.9 can be coming from less effective but more numerous impurities which makes the situation $T \ll |\varepsilon| < 100T$ possible. At the point $\Omega \sim \varepsilon$ the left one of the DoS double-Lorentzian overlaps with the thermal function thus producing a peak in $S(\Omega)$. As Ω further increases, the overlap between the left Lorentzian and the thermal function stays essentially the same but the region where it occurs drifts away to the left from the second Lorentzian which is stationary positioned at $\omega = \varepsilon$. Qualitatively the picture of a linear behaviour of $S(\Omega)$ followed by a peak at $\Omega \sim \varepsilon$ is the same for any relation between γ and T, but the form of the peak is different.

With a purely illustrative purpose we show in Fig.10 a picture corresponding to the following scenario: all the tunneling rates are the same, $\gamma_i = \gamma$, obeying $\gamma \gg T$ (which effectively allows one to put T to zero), and several impurities are uniformly distributed in some interval of energies. All these impurities contribute to the linear behaviour on the left of this interval [the grey area zoomed in the insert a)], while humps might be due to fluctuators with smaller energies weakly coupled to the qubit could not break the general
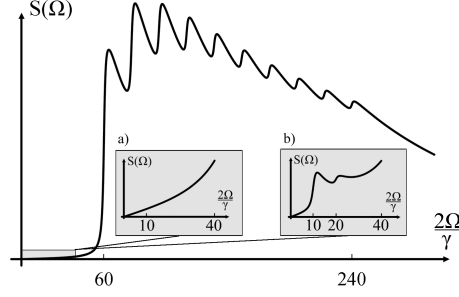
Fig. 10. The noise spectral density $S(\Omega)$ in arbitrary units at $T = 0$ for the case of ten impurities with energies uniformly distributed between $\tilde{\varepsilon} = 60$ and $\tilde{\varepsilon} = 240$. The inserts zoom the bottom left corner (the grey area on the main figure for $\tilde{\varepsilon} \leq 40$) when there is either a) no impurity in this interval or b) two impurities ($\tilde{\varepsilon}_1 = 10$, $\tilde{\varepsilon} = 20$) with coupling constants $v_{1,2}$ 50 times weaker than those for $60 \leq \tilde{\varepsilon} \leq 240$.

linear trend [the grey area zoomed in the insert b)]. The behaviour of $S(\Omega)$ in the grey area qualitatively resembles the experimental data.

7 Conclusions

In these lectures, we have described some essential features of loss of coherence by a qubit coupled to the environment. We have first presented well known semiclassical arguments that relate both decoherence and relaxation to the environmental noise. Then we have shown that models with pure decoherence (when there is no relaxation in qubit states as that part of coupling to the environment that leads to flipping the states is excluded) can be exactly solvable. As an example, we have treated in detail the model of fluctuating background charges [4–7] which is believed to describe one of the most important channels for decoherence for the charge Josephson junction qubit. Following our earlier treatment [7], we have shown that the decoherence rate saturates at 'high' temperatures [4, 5] while becoming linear in T at low temperatures and showing in all regimes a non-monotonic behaviour as a function of the coupling of the qubit to the fluctuating background charges. We have also considered, albeit only perturbatively, the qubit relaxation by the background charges and demonstrated that the quasi-linear behaviour of the spectral density of noise deduced from the measurements of the relaxation rate can be qualitatively explained within this model in the low temperature regime.

References

1. P. W. Shor, SIAM Journal on Computing, **26**, 1484 (1997).
2. L. K. Grover, Phys. Rev. Lett. **79**, 325 (1997).
3. D. P. DiVincenzo and D. Loss, J. Magn. Magn. Mater. **200**, 202 (1999); Phys. Rev. B. **71**, 035318 (2005).
4. E. Paladino, L. Faoro, G. Falci, and R. Fazio, Phys. Rev. Lett. **88**, 228304 (2002).
5. Y. M. Galperin, B. L. Altshuler, and D. V. Shantsev, cond-mat/0312490 (2003).
6. Y. M. Galperin, B. L. Altshuler, J. Bergli, and D. V. Shantsev, Phys. Rev. Lett. **96**, 097009 (2006).
7. A. Grishin, I. V. Yurkevich, and I. V. Lerner, Phys. Rev. B. **72**, 060509 (2005).
8. O. Astafiev, Y. A. Pashkin, Y. Nakamura, T. Yamamoto, and J. S. Tsai, Phys. Rev. Lett. **93**, 267007 (2004).
9. D. P. DiVincenzo, in *Mesoscopic Electron Transport, Vol. 345 of NATO ASI Series E: Applied Sciences*, edited by L. Kouwenhoven *et al.* (Kluwer, Dordrecht, 1997), p. 657.
10. Y. Makhlin, G. Schon, and A. Shnirman, Rev. Mod. Phys. **73**, 357 (2001).
11. Y. Nakamura, Y. A. Pashkin, and J. S. Tsai, Nature **398**, 786 (1999).
12. Y. A. Pashkin, T. Yamamoto, O. Astafiev, Y. Nakamura, D. V. Averin, and J. S. Tsai, Nature **421**, 823 (2003).
13. C. H. van der Wal, A. C. J. ter Haar, F. K. Wilhelm, R. N. Schouten, C. J. P. M. Harmans, T. P. Orlando, S. Lloyd, and J. E. Mooij, Science **290**, 773 (2000).
14. D. Vion, A. Aassime, A. Cottet, P. Joyez, H. Pothier, C. Urbina, D. Esteve, and M. H. Devoret, Science **296**, 886 (2002).
15. Y. Yu, S. Y. Han, X. Chu, S. I. Chu, and Z. Wang, Science **296**, 889 (2002).
16. A. J. Leggett, S. Chakravarty, A. T. Dorsey, M. P. A. Fisher, A. Garg, and W. Zwerger, Rev. Mod. Phys. **59**, 1 (1987).
17. H. P. Breuer and F. Petruccione, *The Theory of Open Quantum Systems* (Oxford University Press, Oxford, 2002).
18. L. Faoro, J. Bergli, B. L. Altshuler, and Y. M. Galperin, Phys. Rev. Lett. **95**, 046805 (2005).
19. G. D. Mahan, *Many-Particle Physics* (Plenum, New York, 1990).
20. J. Rammer and H. Smith, Rev. Mod. Phys. **58**, 323 (1986).